

Control of highly anisotropic electron conductance of tellurene by strain-engineering

Huanhuan Ma,¹ Wei Hu,^{1,*} and Jinlong Yang^{1,†}

¹Hefei National Laboratory for Physical Sciences at Microscale, Department of Chemical Physics, and Synergetic Innovation Center of Quantum Information and Quantum Physics, University of Science and Technology of China, Hefei, Anhui 230026, China

(Dated: November 2, 2019)

I. GEOMETRICAL, ELECTRONIC AND MECHANICAL PROPERTIES OF α -TE

The structure of α -Te is similar to 1-T MoS₂ with $P\bar{3}m1$ symmetry, as shown in Fig. S1 (a), whereas the lattice parameters are $a = b = 4.15$ Å, which are consistent with the previous theoretical work.¹ Two and above-layer α -Te have a sequence of AA stacking, and the mean interlayer distance of α -Te is 2.93 Å. The electronic properties of α -Te are also studied. The PBE + SOC band structure of α -Te is presented in Fig. S1 (b). α -Te is a semiconductor with an indirect bandgap of 0.46 eV within the PBE + SOC scheme (0.71 eV with the HSE + SOC scheme). Using the acoustic phonon limited method,^{2,3} we also calculate the effective mass is $0.11 m_e$ and carriers mobility is 4.06×10^3 cm²·V⁻¹·s⁻¹ of α -Te, which are very consistent with the previous theoretical work.¹

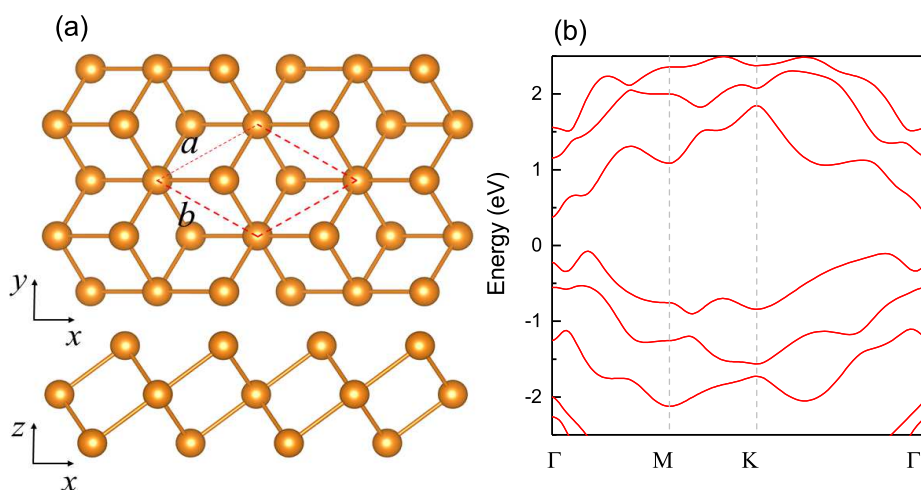


Fig. S1: (a) The top and side views of the relaxed α -Te. (b) Band structure of α -Te, within the PBE scheme with inclusion of the SOC.

We have estimated the mobilities of α -Te under strain. As described in Eq. (2), the calculated mobilities of α -Te at room temperature ($T = 300$ K) according to the biaxial strain is presented in Fig. S2. We find that the mobility of electron under different strain is almost the same with the intrinsic mobility (the difference between the highest mobility and the lowest mobility is about 1000 cm²/v · s). But, the mobility of hole decrease progressively when the strain is changed from -5% to +6%, except for the strain under -4%. It indicate that α -Te is insensitive to strain.

We also calculate the phonon spectrum of α -Te, which is shown in Fig. S3 (a). we can see that the heights of acoustic phonon dispersions of α -Te is 75.44 cm⁻¹, so the Young's modulus is also small. From the orientation-dependent Young's modulus shown in Fig. S3 (b) and (c), we can see the Young's modulus is 57.95 GPa, which confirms our expect. The ideal tensile strength and critical strain of α -Te are also studied, which are shown in Fig. S3 (d). It shows that the ideal strengths of α -Te is up to 39.34 N·m⁻¹ and corresponding tensile strain limits is 20% along diagonal direction.

*E-mail: whuustc@ustc.edu.cn

†E-mail: jlyang@ustc.edu.cn

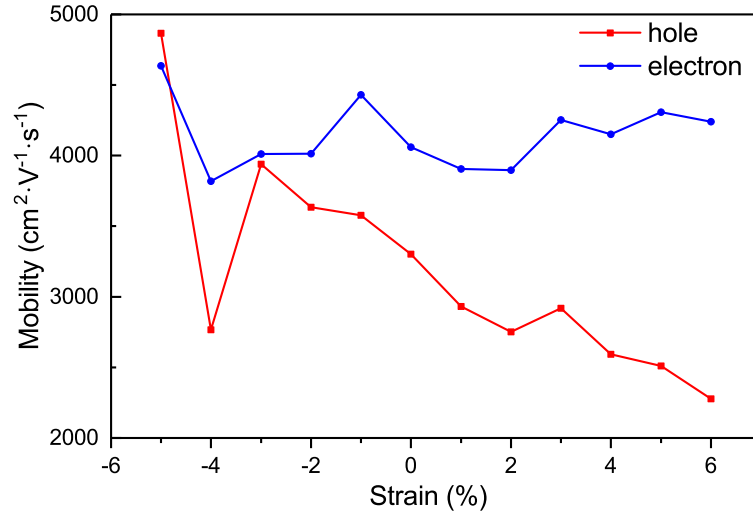


Fig. S2: Hole and electron mobilities of α -Te under biaxial strain at room temperature ($T = 300$ K).

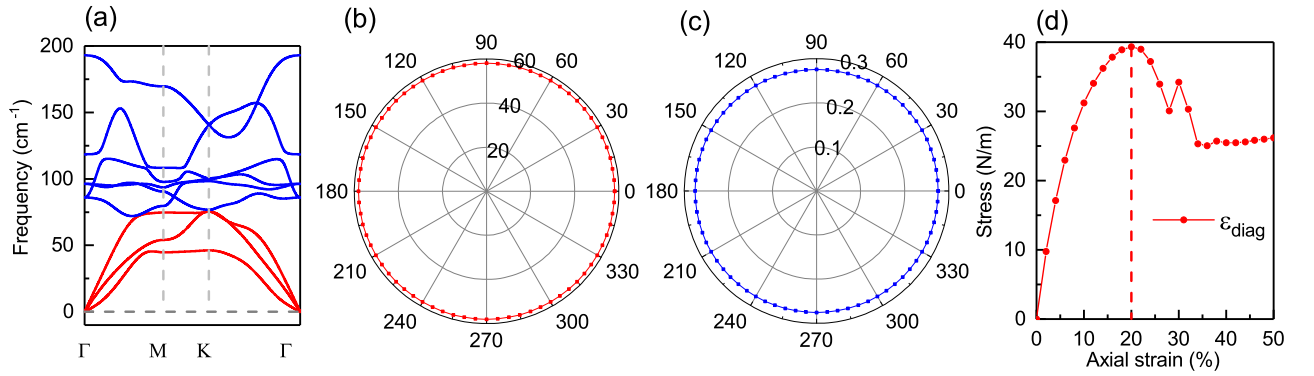


Fig. S3: (a) Phonon band structure of α -Te, where red represents acoustic branch and blue represents optical branch of phonon, respectively. The orientation-dependent (b) Young's modulus $E(\theta)$ in GPa, (c) Poisson's ratio $\nu(\theta)$ of α -Te, respectively. (d) The stress as a function of tensile load for α -Te.

II. PROJECTED BAND STRUCTURE AND DENSITY OF STATES OF INTRINSIC β -TE

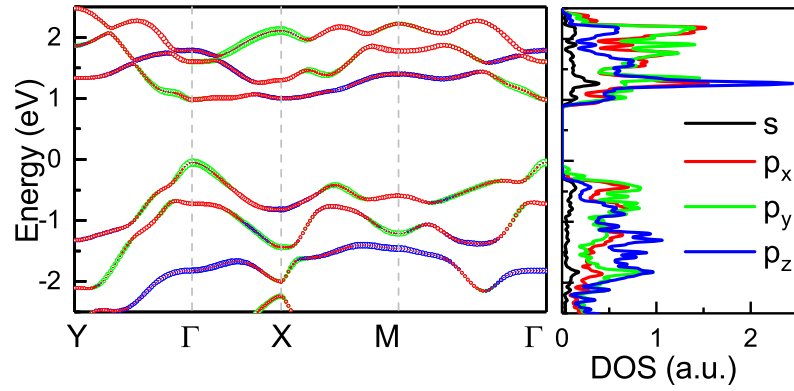


Fig. S4: Projected band structures (pband) and density of states (pDOS) of intrinsic β -Te. Fermi levels are set to zero.

III. PHONON SPECTRUM OF COMMON 2D MATERIALS

Compared with tellurene, we also calculate the phonon spectrum of common 2D materials, which can be seen from Fig. S5.

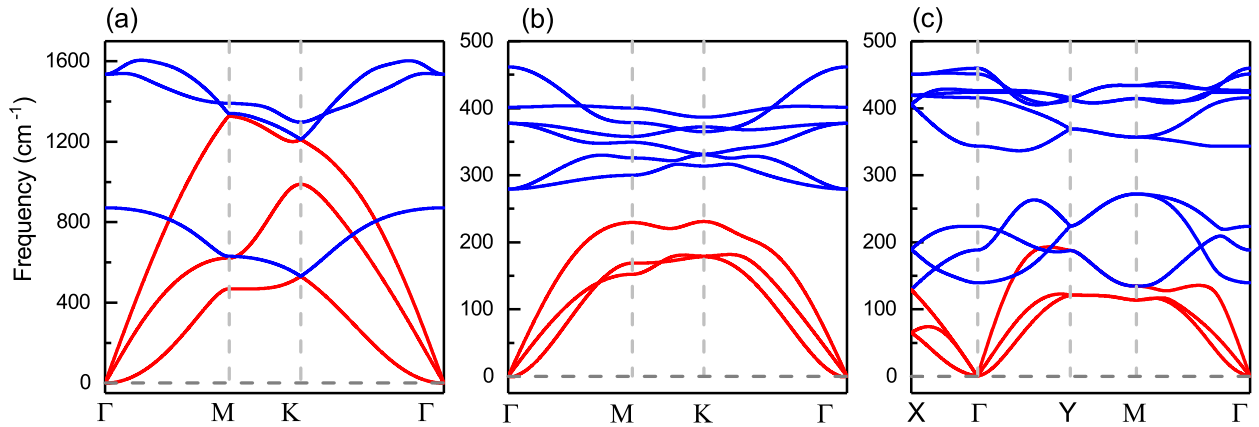


Fig. S5: Phonon spectrum for common 2D materials (a) graphene, (b) MoS₂, and (c) phosphorene, respectively. Red represents acoustic branch and blue represents optical branch of phonon, respectively.

IV. PROJECTED DENSITY OF STATES OF P-ORBIT OF DIFFERENT TE ATOM IN β -TE

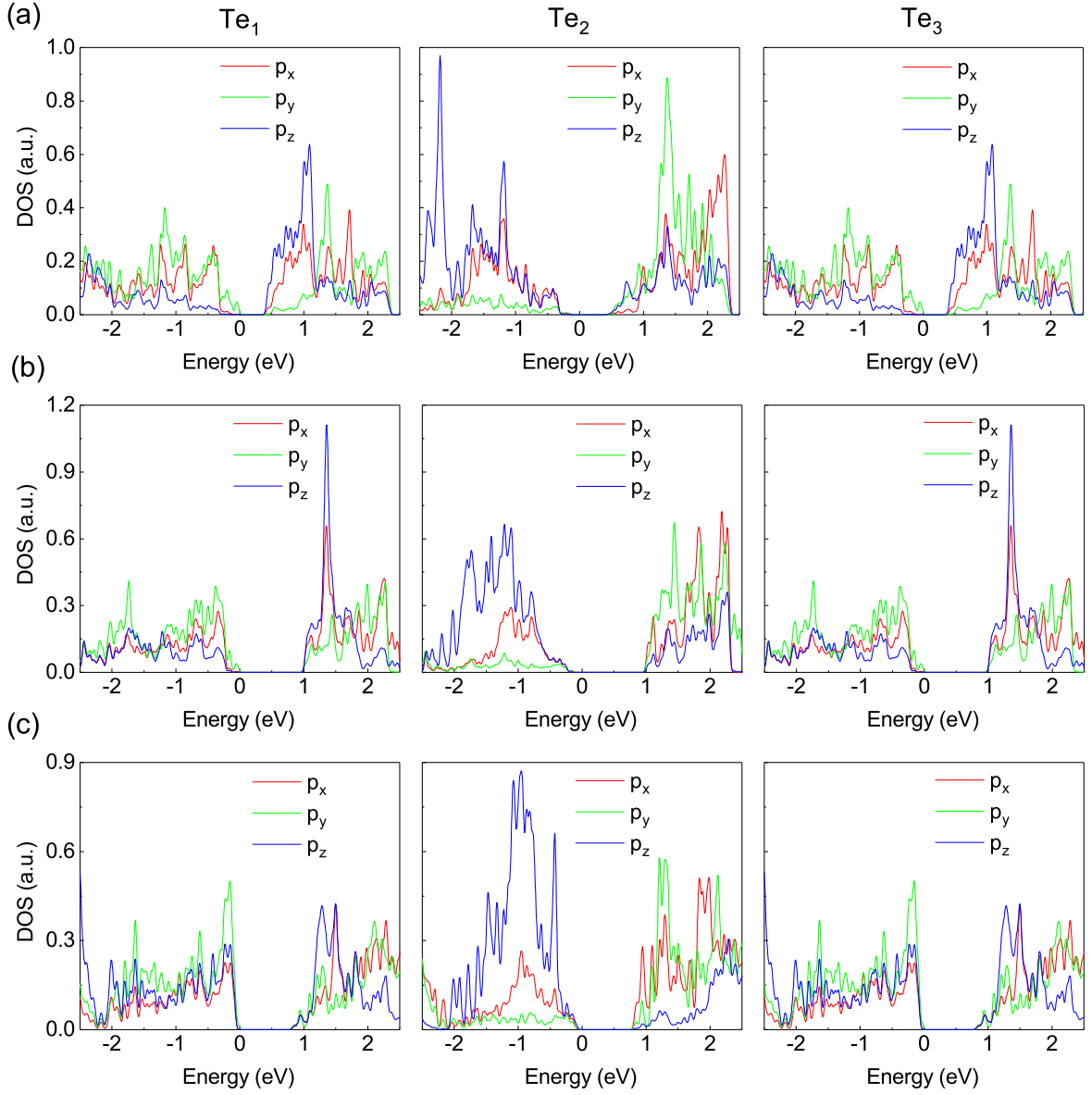


Fig. S6: Projected density of states (pDOS) of p-orbit of different atom Te under (a) -6%, (b) intrinsic and (c) +6% biaxial strain for β -Te. Fermi levels are set to zero.

V. ELASTIC CONSTANTS OF MECHANICAL PROPERTIES

To calculate the orientation-dependent Young's modulus and Poisson's ratio, the elastic constants of d_1 , d_2 , d_3 , Y_{zz} and ν_{zz} are

$$\begin{cases} \nu_{zz} = \frac{C_{12}}{C_{22}} \\ d_1 = \frac{C_{11}}{C_{22}} + 1 - \frac{C_{11}C_{22} - C_{12}^2}{C_{22}C_{66}} \\ d_2 = - \left(2\frac{C_{12}}{C_{22}} - \frac{C_{11}C_{22} - C_{12}^2}{C_{22}C_{66}} \right) \\ d_3 = \frac{C_{11}}{C_{22}} \\ Y_{zz} = \frac{C_{11}C_{22} - C_{12}^2}{C_{22}} \end{cases} \quad (1)$$

where C_{11} , C_{12} , C_{22} , and C_{66} are the elastic stiffness constants, which is presented in Table S1.

Table S1: The calculated elastic stiffness constants for different layered α -Te and β -Te

System	C_{11} (GPa)	C_{22} (GPa)	C_{12} (GPa)	C_{66} (GPa)
mono α -Te	20.67	20.67	5.69	7.48
Double α -Te	31.46	31.46	8.6	11.42
Triple α -Te	37.91	37.91	9.16	14.37
Quad α -Te	37.03	37.03	7.76	14.63
mono β -Te	6.44	14.54	3.82	3.17
Double β -Te	15.40	12.01	3.67	6.43
Triple β -Te	16.51	12.47	3.83	5.94
Quad β -Te	21.81	14.58	4.88	8.31

VI. BAND STRUCTURES OF TELLURENE WITHIN THE HSE06 + SOC SCHEME

To get the accurate band gap, we also perform the hybrid DFT calculations with the HSE06 + SOC functional,^{4,5} as shown in Fig. S7.

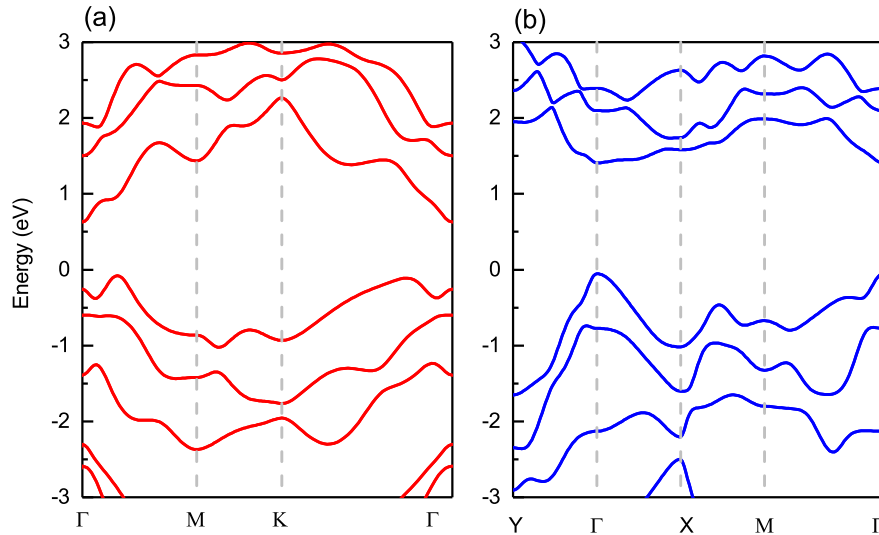


Fig. S7: Band structures of (a) α -Te and (b) β -Te, within the HSE06 scheme with inclusion of the SOC.

VII. INTRINSIC CARRIER MOBILITIES OF TELLURENE

Using the acoustic phonon limited method,^{2,3} we calculate the mobilities of α - and β -Te,

$$\mu_{2D} = \frac{e\hbar^3 C_{2D}}{k_B T m^* m_d (E_1^i)^2} \quad (2)$$

where m^* is the effective mass along the transport direction and $m_d = \sqrt{m_x^* m_y^*}$ is the reduce effective mass. The term E_1^i represents the deformation potential constant of the valence-band minimum (VBM) for hole or the conduction-band maximum (CBM) for electron along the transport direction, defined by $E_1^i = \Delta V_i / (\Delta l / l_0)$. Here, ΔE_i is the energy change of VBM or CBM when tellurene is compressed or dilated from the equilibrium l_0 by a distance of Δl . The term C_{2D} is the elastic modulus of the longitudinal strain in the propagation directions (x or y) of the longitudinal acoustic wave, which can be derived from $2(E - E_0) / S_0 = C(\Delta l / l_0)^2$. Here E and S_0 are total energy and lattice ares, respectively. We use $\Delta l / l_0$ ranging from -1% to +1% to fit the values of C_{2D} and E_1^2 .

We use PBE + vdW-D2 + SOC to calculate the carrier effective mass (m^*), elastic modulus (C_{2D}), deformation potential constant (E_1^i) and mobility of carriers (μ) of α - and β -te are shown in Fig. S8 and S9 and Table S2.

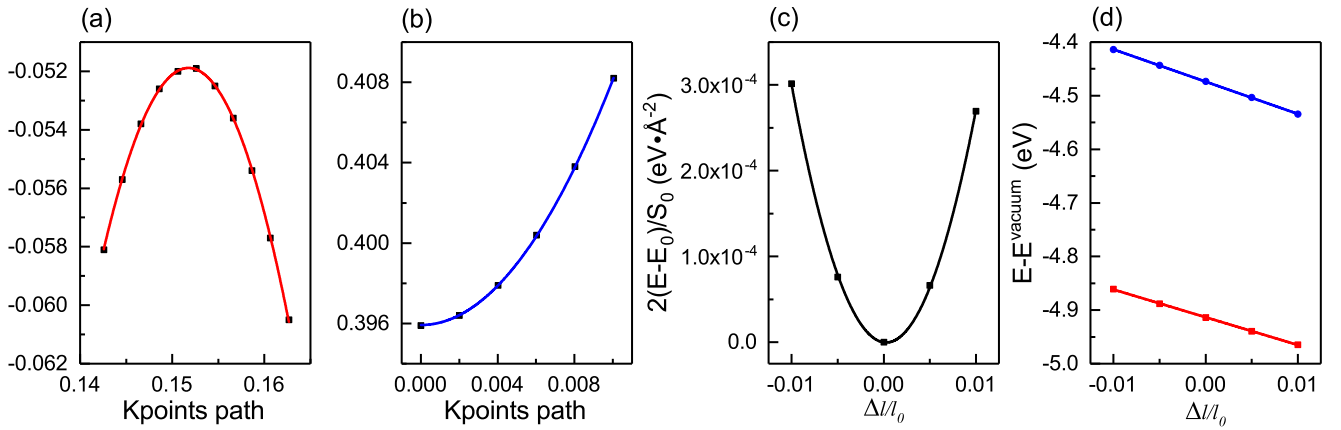


Fig. S8: The intermediate results and curve fitting during mobility calculations of α -Te. (a) VBM is between Γ and M point and (b) CBM near Γ point. (c) total energy changes with respect to deformation. (d) CBM and VBM change with respect to deformation. The red lines are hole, the blue lines are electron.

Table S2: The calculated carrier effective mass (m^*), elastic modulus (C_{2D}), deformation potential constant (E_1^i) and mobility of carriers (μ) of α - and β -Te.

System	m^* (m_e)		C_{2D} ($\text{eV} \cdot \text{\AA}^{-2}$)	E_1^i (eV)		μ ($10^3 \text{ cm}^2 \cdot \text{V}^{-1} \cdot \text{s}^{-1}$)		
	Electron	Hole		CBM	VBM	Electron	hole	
α -Te	0.07	0.12	2.86	6.02	5.17	4.06	3.30	
β -Te	Armchair	1.10	0.34	0.79	3.52	1.25	0.04	2.58
	Zigzag	0.20	0.11	1.77	7.08	7.75	0.13	0.49

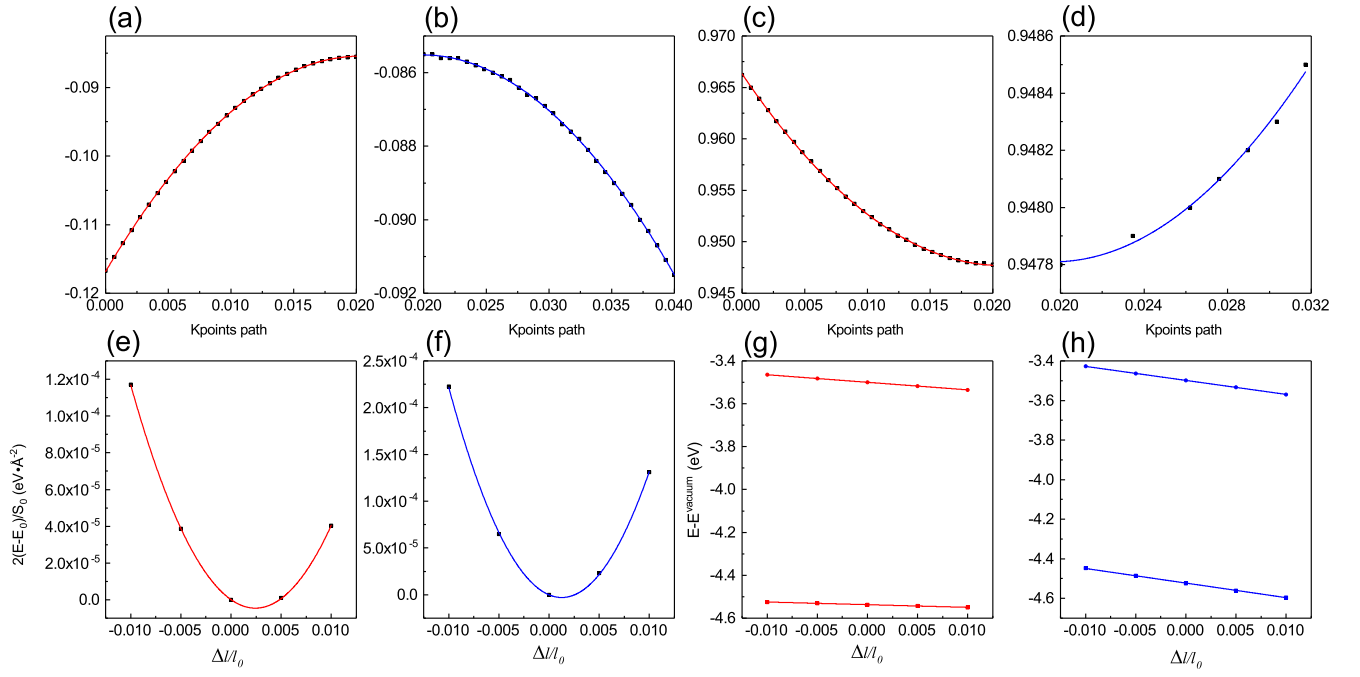


Fig. S9: The intermediate results and curve fitting during mobility calculations of β -Te. (a) and (b) VBM near Γ point. (c) and (d) CBM near Γ point. (e) and (f) total energy change with respect to deformation. (g) and (h) CBM and VBM change with respect to deformation. The red lines are along armchair direction, the blue lines are along zigzag direction.

VIII. COMPRESSED STRAIN-STRESS RELATION

We also calculate the strain-stress relation when the compressed strain is performed in β -Te, as shown in Fig. ???. It shows that the ideal strengths of β -Te are up to $28.42 \text{ N}\cdot\text{m}^{-1}$, $50.18 \text{ N}\cdot\text{m}^{-1}$ and $66.08 \text{ N}\cdot\text{m}^{-1}$ in the armchair, zigzag and diagonal direction, respectively. The corresponding compressed strain limits are 24%, 22% and 22% along armchair, zigzag, and diagonal direction.

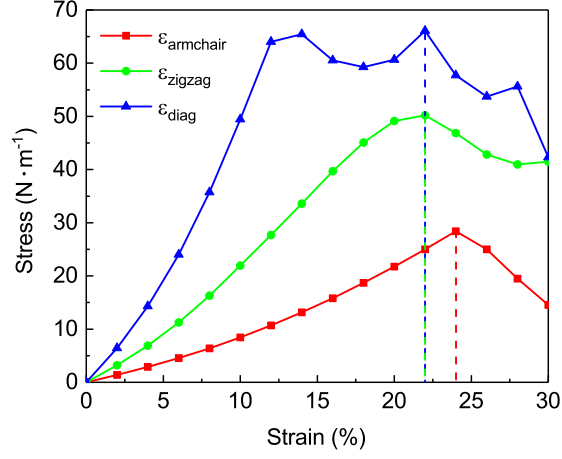


Fig. S10: The stress as a function of compressed load for β -Te.

IX. STACKING ORDER AND MECHANICAL PROPERTIES OF MULTILAYER TELLURENE

The stacking order of α - and β -Te are also studied in this work. We find that two- and above-layer α -Te have a sequence of AA stacking. The three-layer α -Te is shown in Fig. S11 (a). Two-layer β -Te has a sequence of AB stacking as bulk tellurium. The three- and four-layer β -Te structure take the stacking sequence of ABA and ABAB, respectively. The three-layer β -Te is shown in Fig. S11 (b). We also calculate the bandgap as a function of number of layers for α -Te and β -Te, which is shown in Fig. S12.

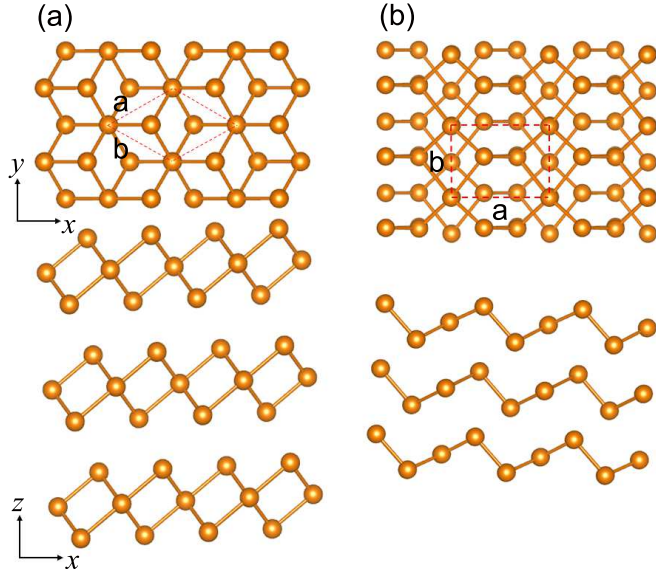


Fig. S11: The top and side views of the relaxed (a) three-layer α -Te and (b) three-layer β -Te.

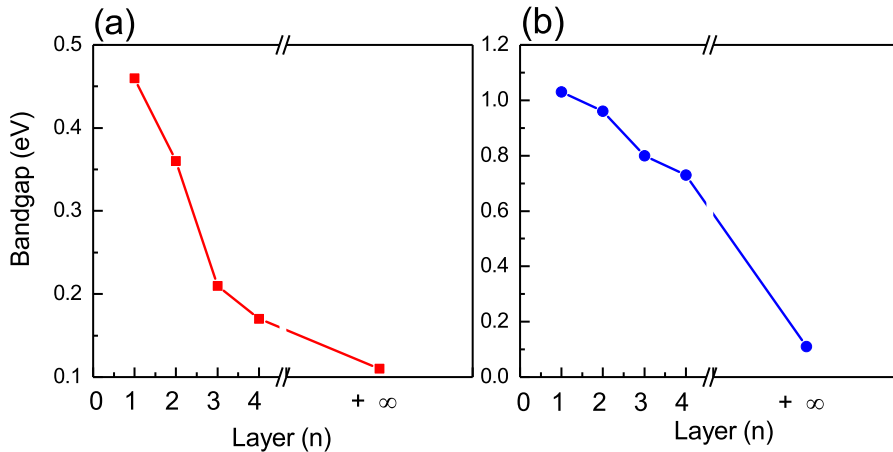


Fig. S12: The bandgap as a function of number of layers for (a) α -Te and (b) β -Te, within the PBE scheme with inclusion of the SOC.

Using the first-principles methods, we calculate the stress which has to be modified to avoid the force being averaged over the entire simulation cell including the vacuum slab.⁶ In order to compare Young's modulus among different layered-structures, the length along z direction is rescaled by $n\bar{h}$, where \bar{h} is mean interlayer distance and n denotes the number of layer. The mean interlayer distance is shown in Table S3.

The mechanical properties of α - and β -Te also have also been studied in this work, which are shown in Fig. S13. Young's modulus and Poisson's ratio of multilayer β -Te are different from monolayer β -Te due to the structure of

multilayer is similar to bulk structure of Te, can be seen from Fig. S11.

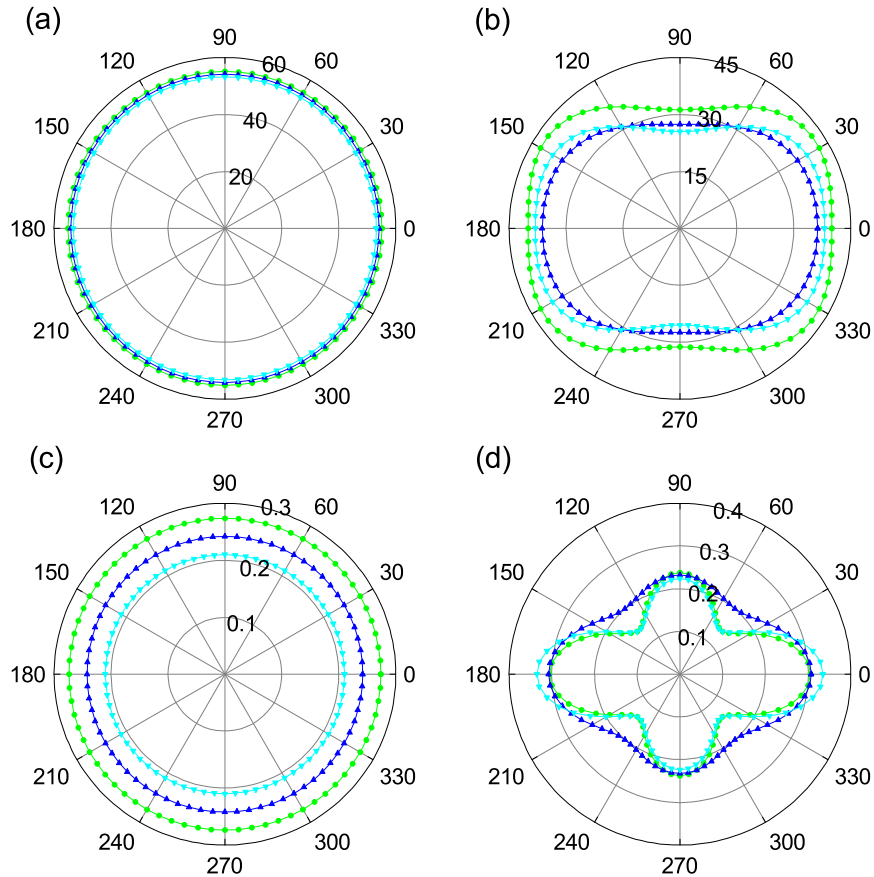


Fig. S13: The orientation-dependent (a) and (b) Young's modulus $E(\theta)$ in GPa, (c) and (d) Poisson's ratio $\nu(\theta)$ of multilayer α - and β -Te, respectively. Green, blue and cyan represent bilayer, 3- and 4-layer, respectively.

Table S3: The calculated elastic stiffness constants for different layered α -Te and β -Te

System	stacking order	\bar{h} (\AA)	lattice constants (\AA)	
			a	b
monolayer α -Te	A	/	4.15	4.15
Double α -Te	AA	2.95	4.16	4.16
Triple α -Te	AAA	2.92	4.17	4.17
Quadruple α -Te	AAAA	2.92	4.17	4.17
monolayer β -Te	A	/	5.49	4.17
Double β -Te	AB	1.81	5.79	4.24
Triple β -Te	ABA	1.79	5.88	4.27
Quadruple β -Te	ABAB	1.74	5.93	4.30

X. OTHER FACTORS INFLUENCE THE ELECTRICAL DIRECTION

As discussion in Section-2, in addition to effective mass can influence the carrier mobility, there also has other two parameters (elastic modulus (C_{2D}) and deformation potential constant (E_1^i)) can influence the mobility of electron. As we see from Fig. S14 (a), the ratio of elastic modulus in the zigzag and armchair direction is change slightly, so elastic modulus can slightly influence electronic mobility. On the another hand, we find that the ratio of deformation potential constant of electron along zigzag and armchair direction is similar to the Fig. S14 (b), so the deformation potential constant also plays an important role in the rotation of anisotropy.

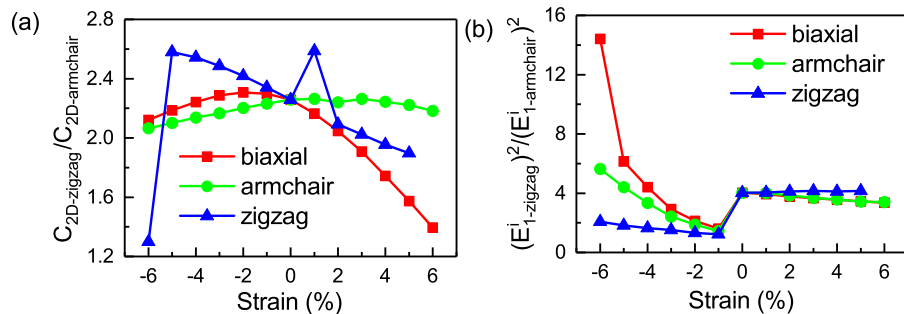


Fig. S14: (a) The curve of ratio of elastic modulus (C_{2D}) in the zigzag and armchair direction under biaxial, uniaxial armchair and zigzag strain. (b) The curve of ratio of deformation potential constant (E_1^i) of electron along zigzag and armchair direction under biaxial, uniaxial armchair and zigzag strain.

XI. EFFECTIVE MASSES TENSOR AND BAND STRUCTURE OF TELLURENE UNDER STRAIN

In order to explore the rotation of anisotropic conductance of β -Te, the electron effective masses tensor of β -Te is also calculated under 6% tensile strain along diagonal direction as shown in Fig. S15. The effective mass is $1.24 m_e$ along the armchair direction while it is $0.12 m_e$ along the zigzag direction. To calculate the mobilities of tellurene, we study the band structures of α - and β -Te under strain, which are presented in Fig. S16, S17, S18 and S19. We can find that the band structure of α -Te is insensitive to strain (expect for -6% strain along diagonal direction). The bandgap and effective mass of α -Te under strain are shown in Fig. S20 (a) and (b). But β -Te experiences an indirect-direct transition when strain is applied. The bandgap and effective mass of β -Te under strain are also presented in Fig. S20 (c), (d), (e) and (f). The band structure of β -Te under 5% strain along zigzag direction exhibits a slight indirect band gap and the energy difference between the bottom of the conduction band and the local minimum at the X point is vary small (less than 10 meV). Therefore, given this small and delicate energy difference, we regard β -Te under 5% strain along zigzag direction as a direct-gap semiconductor in this work. Finally, We used the advanced hybrid functional HSE06 + SOC to calculate the band structures of α - and β -Te under strain, and the results are presented in Fig. S21. Comparing the HSE06 +SOC predicted band structures with PBE + SOC, one can conclude that both methods give the consistent results of the strain effects on the band structures.

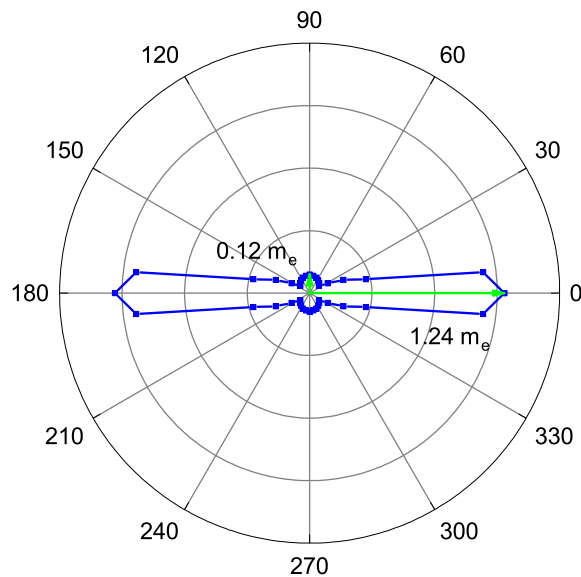


Fig. S15: Electron effective masses tensor according to spatial direction of 6% tensile strained β -Te. The length of blue arrow represents absolute values of effective mass

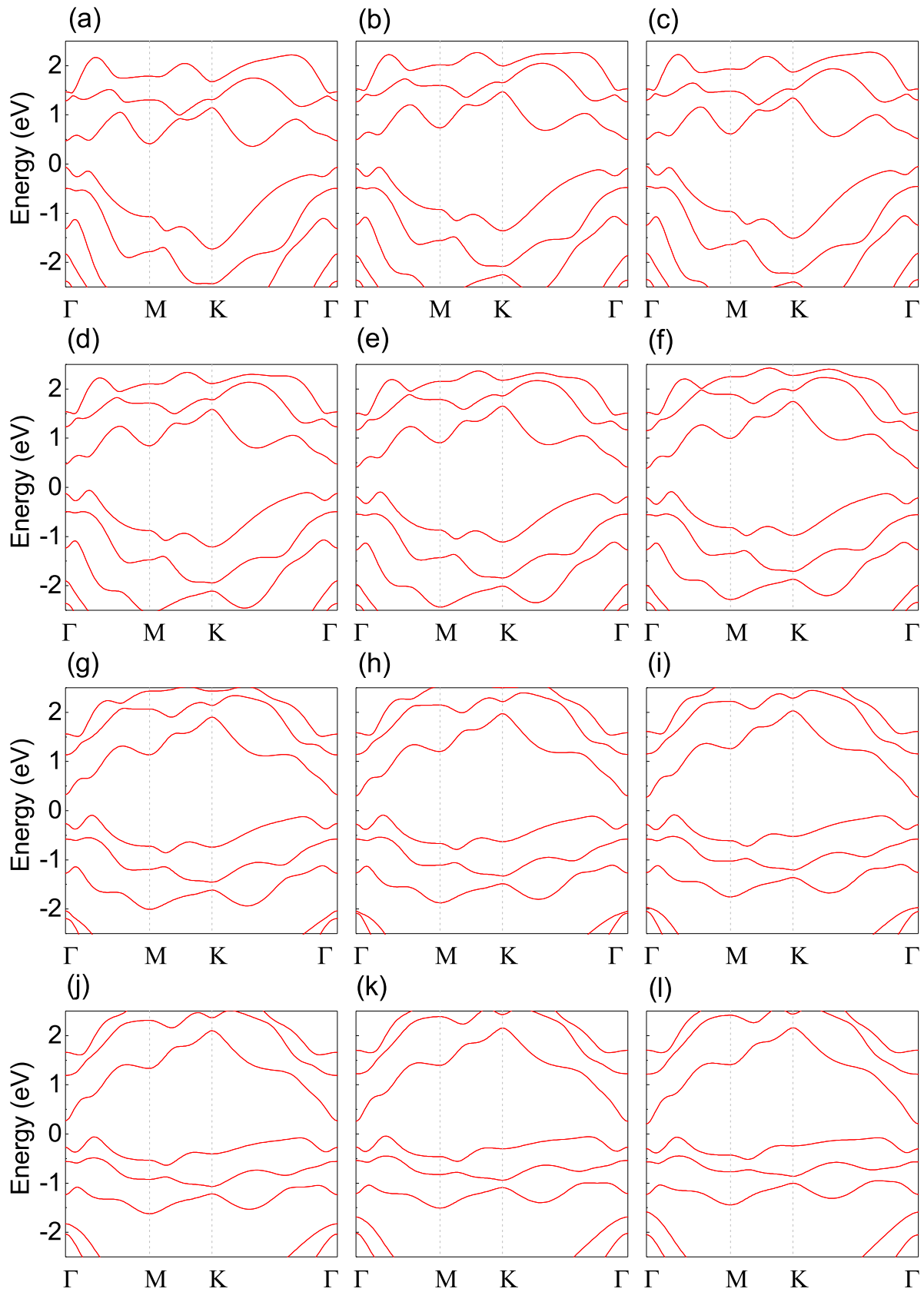


Fig. S16: The strain ϵ_{diag} (along the diagonal direction) manipulate the band structure transition in α -Te within the PBE scheme with inclusion of the SOC. The strain ranges from -6% to -1% in (a) to (f), and from 1% to 6% in (g) to (l).

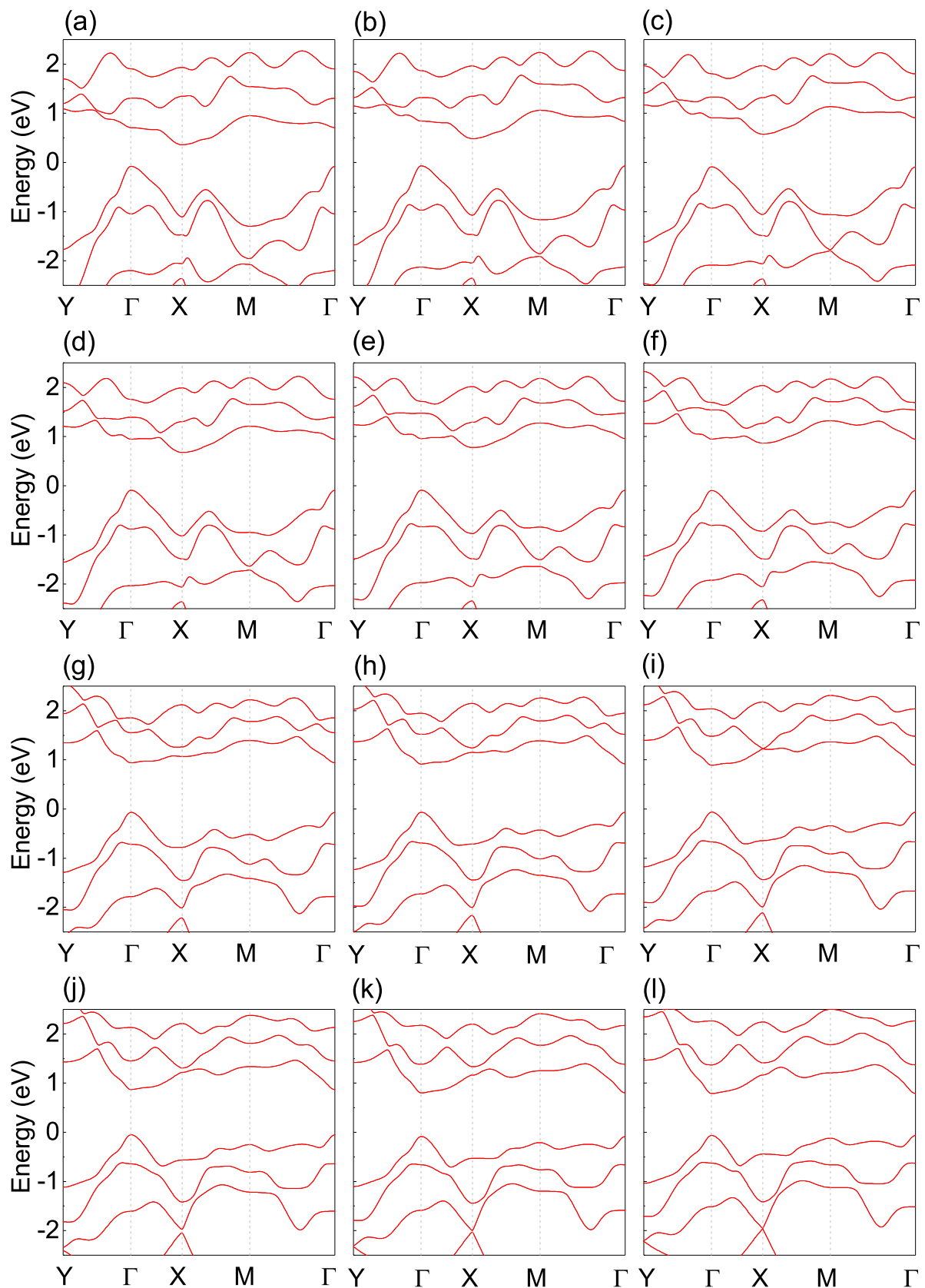


Fig. S17: The strain ϵ_{diag} (along the diagonal direction) manipulate the band structure transition in β -Te, within the PBE scheme with inclusion of the SOC. The strain ranges from -6% to -1% in (a) to (f), and from 1% to 6% in (g) to (l).

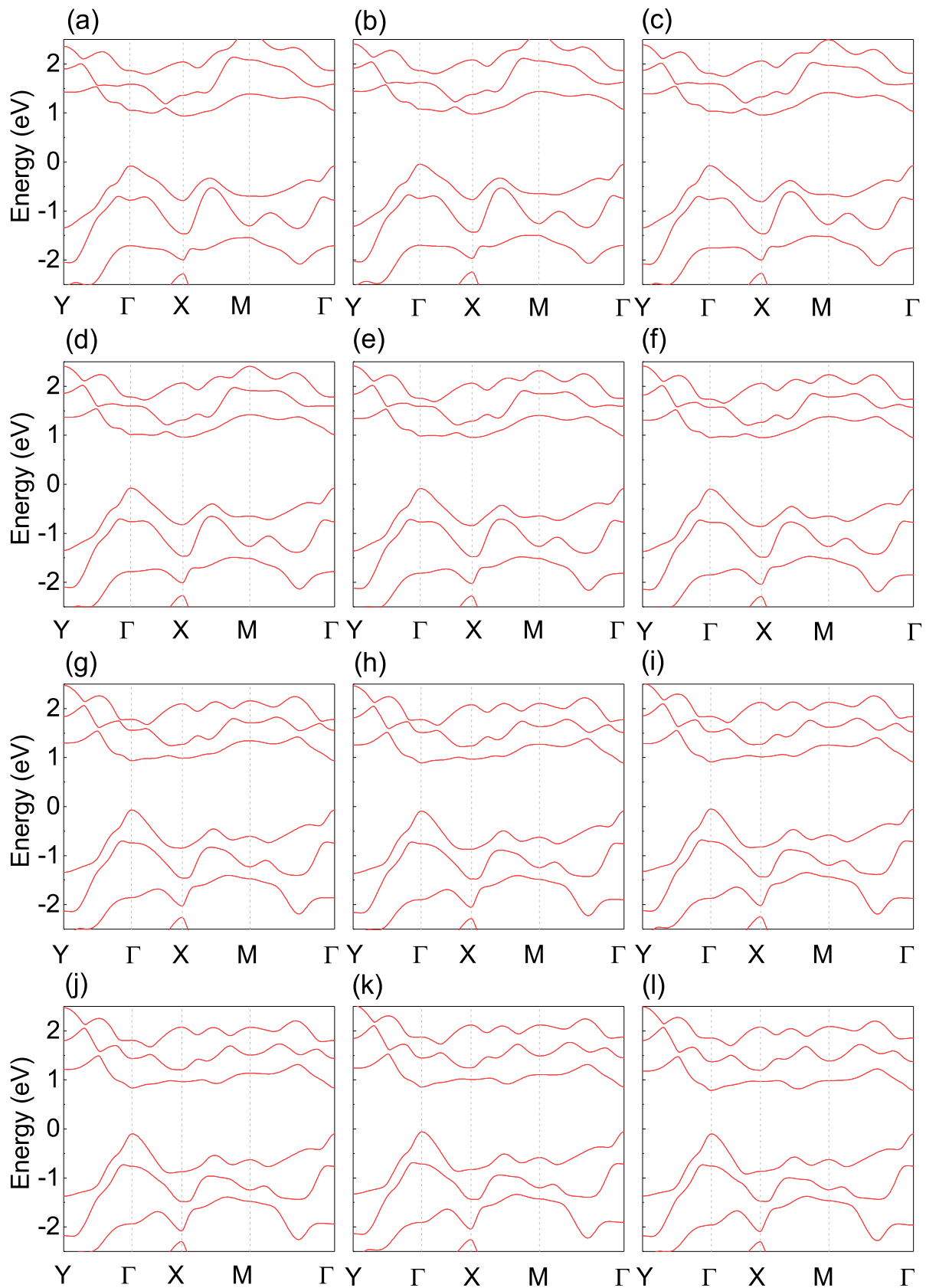


Fig. S18: The strain ϵ_x (along the armchair direction) manipulate the band structure transition in β -Te, within the PBE scheme with inclusion of the SOC. The strain ranges from -6% to -1% in (a) to (f), and from 1% to 6% in (g) to (l).

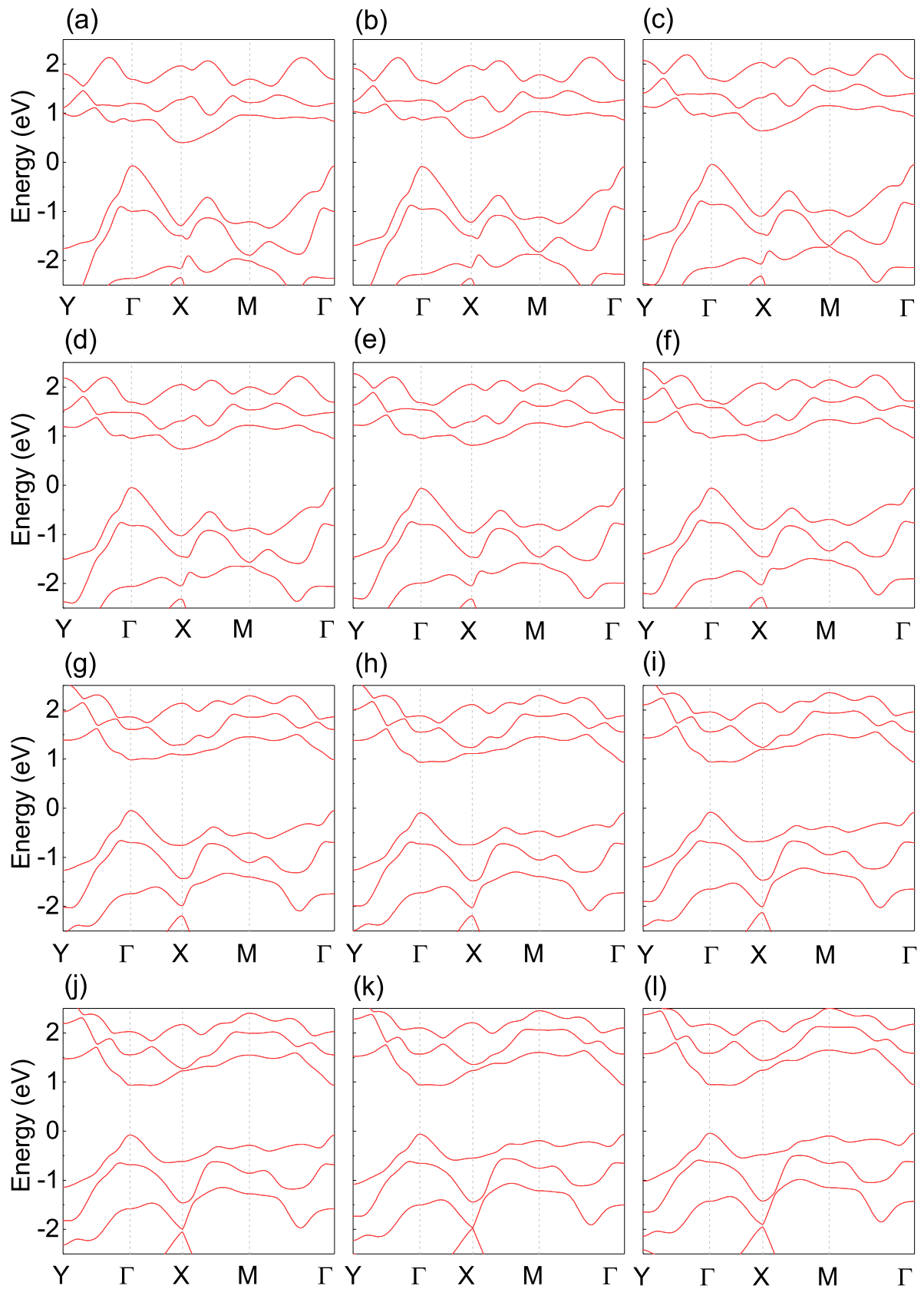


Fig. S19: The strain ϵ_y (along the zigzag direction) manipulate the band structure transition of β -Te, within the PBE scheme with inclusion of the SOC. The strain ranges from -6% to -1% in (a) to (f), and from 1% to 6% in (g) to (l).

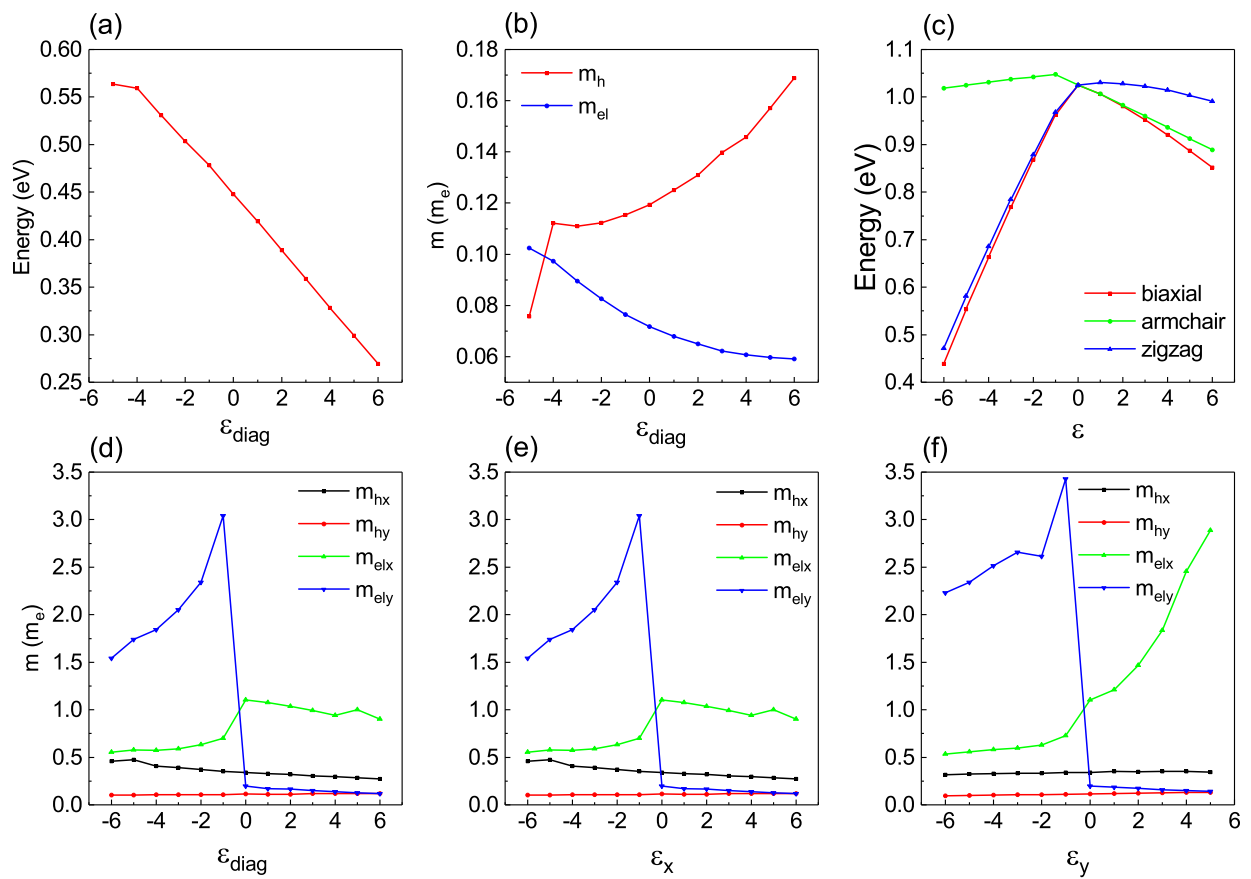


Fig. S20: (a) Bandgap and (b) effective mass of α -Te under strain. (c) Bandgap vs strain of β -Te. Effective mass of electron and hole when the strain applied in β -Te along (d) diagonal, (e) armchair and (f) zigzag direction.

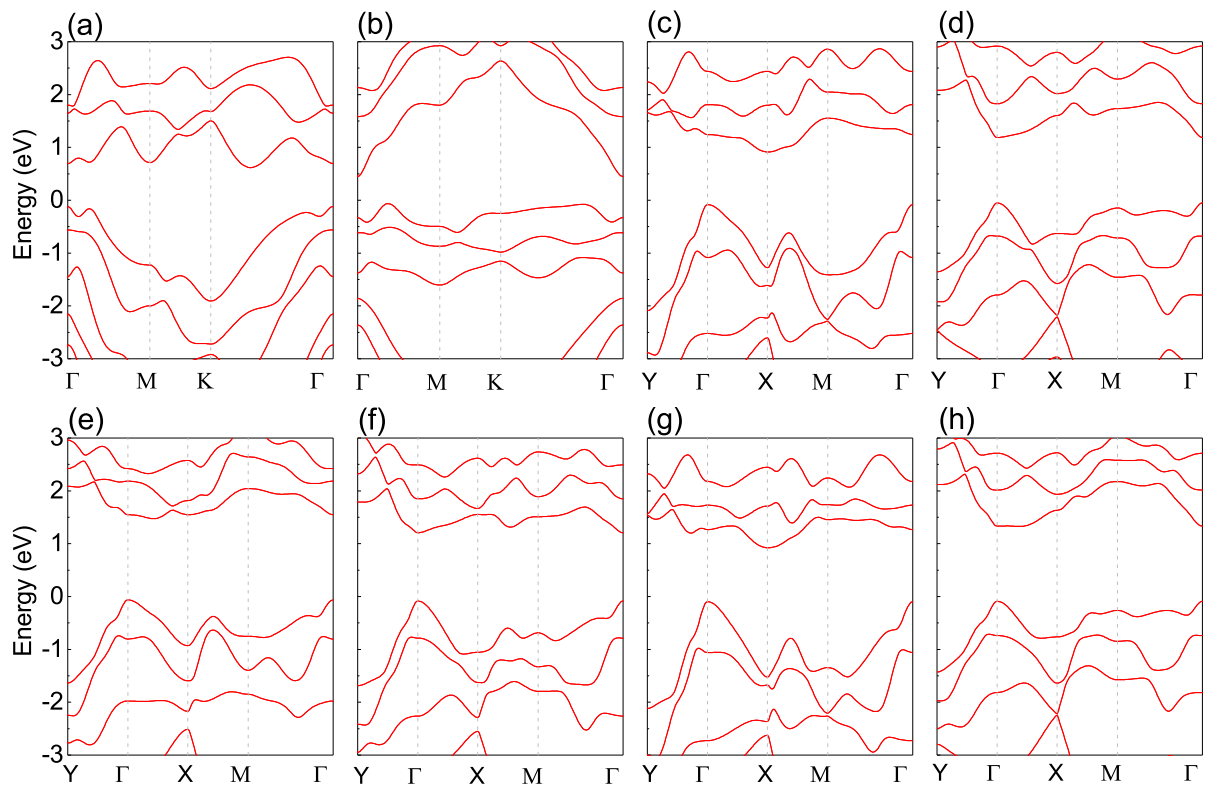


Fig. S21: The band structure of α -Te within HSE06 + SOC scheme, when the (a) -6% and (b) 6% strain applied along diagonal direction, respectively. The band structure of β -Te within HSE06 + SOC, when the -6% strain applied along (c) diagonal, (e) armchair and (g) zigzag direction, respectively, while +6% strain applied along (d) diagonal and (f) armchair direction. (h) Band structure of 5% strain apply in the β -Te along zigzag direction.

-
- [1] Z. Zhu, X. Cai, S. Yi, J. Chen, Y. Dai, C. Niu, Z. Guo, M. Xie, F. Liu, J.-H. Cho, et al., Phys. Rev. Lett. **119**, 106101 (2017).
- [2] J. Bardeen and W. Shockley, Phys. Rev. **80**, 72 (1950).
- [3] S. Bruzzone and G. Fiori, Appl. Phys. Lett. **99**, 222108 (2011).
- [4] J. Heyd, G. E. Scuseria, and M. Ernzerhof, J. Chem. Phys. **118**, 8207 (2003).
- [5] A. V. Krugau, O. A. Vydrov, A. F. Izmaylov, and G. E. Scuseria, J. Chem. Phys. **125**, 224106 (2006).
- [6] Q. Wei and X. Peng, Appl. Phys. Lett. **104**, 251915 (2014).